DOI: 10.31534/engmod.2026.2.ri.01v
Original scientific paper
Received: 16.10.2025.
This article is an open access article distributed under the terms and conditions of the Creative Commons Attribution (CC BY) license.

Influence of Corrosion on the Fatigue Behaviour of 5083 Lap-Welded Joints

Tomislav Matić[(1,*)], **Dražen Kustura**[(1)], **Ivan Peko**[(1)], **Francisko Lukša**[(2)]

(1) *Faculty of Science, University of Split, Ruđera Boškovića 33, Split, CROATIA*
e-mails: tmatic@pmfst.hr; dkustura@pmfst.hr; ipeko@pmfst.hr

(2) *Faculty of Maritime Studies, University of Split, Ruđera Boškovića 37, Split, CROATIA*
e-mail: fluksa@pfst.hr

* *Corresponding author*

SUMMARY

The design and durability of welded aluminium structures, commonly used in the marine, aerospace, and automotive industries, require a thorough understanding of their mechanical performance under cyclic loading and various environmental conditions, including corrosion. Aluminium–magnesium alloys (such as 5083) are widely used in marine applications due to their favourable strength-to-weight ratio and inherent corrosion resistance. However, prolonged exposure to harsh environments inevitably leads to corrosion-induced damage, which negatively affects the fatigue strength of welded joints.

This study investigates the influence of corrosion on the fatigue behaviour of lap-welded 5083 aluminium joints through a controlled experimental programme. Fatigue tests were conducted on two groups of specimens: one with corrosion damage and the other uncorroded. Comparative analysis of the fatigue life data indicates a reduction in fatigue strength attributable to corrosion. Specifically, the fatigue strength at $2{\cdot}10^6$ cycles is reduced by approximately 50% or 38%, depending on whether the nominal stress approach or the notch stress approach is used for fatigue assessment.

KEYWORDS: *5083 aluminium alloy; accelerated pre-corrosion; pitting; bending fatigue; notch stress approach.*

1. INTRODUCTION

Between 2000 and 2024, global primary aluminium production nearly tripled, increasing from approximately 24.5 million tonnes to about 72 million tonnes. This growth reflects the rising demand across all major aluminium-consuming sectors, including transportation (automotive, aerospace, rail, etc.), marine shipping, construction, packaging, and electrical applications [1]. This increase is primarily attributable to the properties of aluminium alloys such as a favourable

strength-to-density ratio, good corrosion resistance, ease of forming, high thermal conductivity, good electrical conductivity, and non-magnetic behaviour [2, 3].

In shipbuilding, aluminium alloys are used for constructing ship superstructures (to achieve greater stability or allow larger superstructures), interior ship architecture, and various auxiliary equipment and components (such as masts and funnels). Smaller vessels and structures are often built entirely from aluminium alloys, particularly lifeboats, yachts, and catamarans [4].

In the manufacture of ships and other maritime structures, individual components are joined by welding. These welded structures are subjected to dynamic loading and environmental influences, among which corrosion is the most significant. Aluminium alloys 5083, 5084, and 5456 are commonly used in shipbuilding due to their good corrosion resistance [5]. Over time, however, even these alloys experience corrosion-related degradation. Consequently, a thorough understanding of component behaviour under fatigue loading and corrosive conditions is required for the optimal design of such structures.

The effect of seawater on aluminium–magnesium alloys leads to measurable damage that varies with the type and duration of exposure. Ailor [6] reports corrosion rates of 0.3556–1.2954 micrometres per year (*μm/yr*), with maximum pit depths of 1.829 *mm* after 10 years of exposure under semi-aqueous conditions. Under full immersion, corrosion rates of 0.914–1.6256 *μm/yr* and pit depths of up to 3.327 *mm* were observed (Table 1). In the same study, tensile strength losses of 3.7–5.2% and elongation losses of 6–27% were reported after 10 years of exposure.

Nwoye et al. [7] report corrosion penetration depths in aluminium–manganese alloys exposed to seawater for 7 days. When the corrosion rate increased from 10.4 to 15.7 *μm/yr*, the penetration depth was 10.123 *μm*, whereas a decrease in the corrosion rate from 15.7 to 6.2 *μm/yr* resulted in a penetration depth of 18.240 *μm*. Le [8] states that after 16 years of complete immersion in a low-salinity environment, a severe corrosion morphology develops, a phenomenon attributed to electrolyte effects.

Table 1 *Results of pitting corrosion in aluminium alloys after 10 years of exposure to seawater in the leaching zone and under complete immersion [6]*

Aluminium Alloy	*Leaching zone (maximum pitting depth), mm*	*Complete immersion in the sea, (maximum pitting depth), mm*
5086-O	*0.689*	*0.460*
5083-O	*0.965*	*0.610*
5456-O	*1.740*	*3.327*
5456-H321	*1.829*	*1.151*

Goddard et al. [9] observed that the maximum pit depth in three 5000-series aluminium alloys (5052, 5056, and 5083) immersed in seawater reached 0.18 *mm* after 5 years and increased to 0.86 *mm* after 10 years. These results indicate that seawater can cause pitting, measurable corrosion rates, and moderate mechanical degradation in aluminium–magnesium alloys. Variations in immersion conditions (half immersion versus full immersion) and differences in electrolyte environments influence both the quantitative extent and the type of corrosion damage observed, as documented in studies of similar alloys such as 5083.

Pantelakis and Kermanidis [10] reported that pre-corroded aluminium specimens exhibited changes in fatigue behaviour, as indicated by qualitative metallographic analysis; however, they did not provide numerical measurements of the extent of corrosion or the associated reduction in fatigue strength. Heuler and Birk [11] investigated aluminium components from the

automotive industry tested under variable-amplitude loading in a 3.5% sodium chloride solution. Their results described general effects on fatigue performance without specifying quantitative reductions in strength.

Several studies on corroded aluminium welds employed pre-corrosion exposure times ranging from 10 to 1000 hours in a 3.5% NaCl solution, focusing on friction stir welded AA2024-T3 joints [12, 13, 14, 15]. However, these studies reported only qualitative observations, stating that corrosion significantly decreased fatigue life, without providing percentage reductions, fatigue strength values in MPa, or comparative S–N curve parameters.

Hailiang Wu et al. [16] further demonstrated that different corrosive environments (e.g., NaCl and $NaHSO_3$ solutions) can have varying impacts on mechanical properties, with certain conditions causing reductions of up to 50% in elongation and fatigue life.

Only one source, Yuqiang Chen et al. [17], provided explicit numerical comparisons, reporting fatigue life reductions of 84.5% after 3 days, 90.7% after 7 days, 93.1% after 15 days, and 95.7% after 30 days of corrosion exposure for 5083-H111/6005A-T6 dissimilar welded joints in a 3.5% NaCl + 0.01 *mol/L* $NaHSO_3$ solution. However, these results pertain specifically to dissimilar aluminium alloy joints rather than homogeneous 5083 welds, and the aggressive mixed-ion corrosion environment may represent a worst-case scenario compared to natural seawater exposure.

Jie et al. [18] investigated load-carrying cruciform joints made of Q345qC steel plates with a thickness of 16 *mm* and found that artificial pits reduced the fatigue strength by 24–31% at stress ranges of 140–180 *MPa*.

Overall, these studies consistently indicate that corrosion-induced pitting, whether natural or artificial, promotes crack initiation at the weld toe and degrades fatigue performance under comparable stress conditions.

The S–N curve method is widely used in the design of welded joints made from aluminium alloys. The nominal stress range is used to determine permissible stresses [19, 20, 21]. With this approach, the effects of weld geometry and structural discontinuities are considered indirectly, as these factors are incorporated into the S–N curves. The FAT22 S–N curve is used, for example, in the design of lap-welded joints [20]. According to the recommendations of the International Institute of Welding (IIW), stresses should be calculated using a plate width equal to the weld length [20]. Alternatively, fatigue analysis may be performed using the notch stress approach. While the nominal stress approach is suitable for conventional design scenarios, the notch stress approach is preferred for critical or non-standard joints where localised geometric effects are significant, although it requires greater modelling accuracy and validation.

The notch stress is the local stress within a component arising from geometric discontinuities and weld seam characteristics, assuming linear-elastic material behaviour [22, 23]. This increased stress level is quantified by the notch stress concentration factor (K_t), defined as the ratio of the notch stress to the nominal stress. The value of K_t can be determined through detailed analysis of the weld geometry, typically using finite element (FE) or boundary element (BE) methods. In FE simulations of aluminium alloy welds, the notch stress is calculated by modelling the sharp transitions of the actual weld profile using specified reference radii. As described by Baumgartner et al. [24], the appropriate reference radius for evaluating weld toe failures depends on the plate thickness: $r_{ref} = 1\ mm$ for $t \geq 5\ mm$, $r_{ref} = 0.3\ mm$ for $1.5\ mm \leq t \leq 10\ mm$, and $r_{ref} = 0.05\ mm$ for $t < 5\ mm$. An identical proposal is included in the IIW Recommendations for Fatigue Design of Welded Joints and Components [20]. The fatigue

strength classes FAT71, FAT95, and FAT160 are used to evaluate failures at the weld toe with opening angles between 90° and 150°, corresponding respectively to reference radii of 1 mm, 0.3 *mm*, and 0.05 *mm* used in the modelling process [24].

The FAT classes represent standardised fatigue strength levels expressed as stress ranges based on the maximum principal stress hypothesis and are associated with specific survival probabilities, typically 97.7% at a statistical confidence level of 95% [22]. These values are derived for the as-welded condition and reflect the effects of elevated residual tensile stresses. The FAT classes are particularly valuable for assessing fatigue behaviour in real welded structures, where manufacturing processes and assembly constraints generate significant residual stresses in fatigue-critical regions [20].

In cases where structures exhibit low residual stresses or have been stress relieved, the fatigue strength specified for the as-welded condition may be increased. This increase is achieved by applying a correction factor that accounts for the mean stress level, typically characterised by the stress ratio *R*. The increase factor *f(R)* is defined as follows [25]:

$$\begin{gathered} f(R) = 1.3, for\ R\ \leq -1 \\ f(R) = 0.9 - 0.4 \cdot R, for -1 \leq R \leq -0.25 \\ f(R) = 1, \text{for } R \geq -0.25 \end{gathered} \quad \textbf{(1)}$$

The fatigue strength values provided apply to non-corrosive environments and assume adequate protection against atmospheric corrosion.

This paper investigates the effect of corrosion damage on the fatigue behaviour of lap-welded joints made from aluminium alloy 5083. The fatigue lives of uncorroded and previously corroded lap-welded joints are compared. Fatigue analysis is performed using both the nominal and the notch stress approaches. The results for uncorroded lap-welded joints are compared with the recommended S–N curves for design purposes.

2. TEST SPECIMENS

The lap-welded test specimens were fabricated from aluminium alloy 5083 sheets with a thickness of 3 *mm*. The welding parameters were as follows:

- Welding procedure: MIG welding
- Welding current: 175 *A*
- Welding voltage: 18 *V*
- Parent metal: 5083, 3 *mm* thick
- Filler metal: 5056, diameter 1.2 *mm*

Variations in material hardness resulting from the welding process were measured. The Vickers hardness values were 80–83 *HV* in the parent metal and 63–66 *HV* in the heat-affected zone.

The specimen geometry is shown in Figure 1. A tapered design was chosen to achieve an approximately constant nominal stress along the entire length of the specimen. The longitudinal axes of the test specimens are parallel to the rolling direction of the plate. The fillet weld dimensions, welding techniques, and associated process parameters were applied in accordance with the defined standard specifications [26, 27]. The weld seams underwent dimensional measurements, visual inspection, and ultrasonic testing as a pre-screening quality-control step. Dimensional measurements were used to verify a fillet weld leg length of 3 *mm*, and specimens

with noticeable deviations, welding-induced distortion, or misalignment were excluded. Visual and ultrasonic inspections were performed to identify surface and internal weld irregularities, particularly lack of fusion or incomplete penetration. These inspections were conducted solely for specimen selection, and individual inspection results were not recorded. In total, 30 test specimens were produced.

Eight specimens were subjected to corrosion according to ASTM-G48 to produce pre-corroded specimens for mechanical fatigue testing. This test method is primarily used to evaluate the pitting and crevice corrosion resistance of stainless steels and related alloys using a ferric chloride solution. The use of a ferric chloride solution for aluminium corrosion tests can cause aggressive and unrealistic damage that does not correspond to damage occurring under maritime operating conditions. For this reason, test parameters such as solution concentration, temperature, and exposure time must be carefully optimised to avoid excessive or unrepresentative attack. The specimens were therefore corroded for 72 hours in a ferric chloride solution (100 g of ferric chloride in 900 mL of distilled water), ensuring a solution-to-exposed-surface ratio of 20 mL/cm^2 to prevent saturation of the corrosion product. The temperature of the solution was maintained at 22 ± 2°C. As a result of corrosion, an increase in surface roughness and pitting was observed (Figure 2). The surface roughness values for specimens with and without corrosion are shown in Table 2.

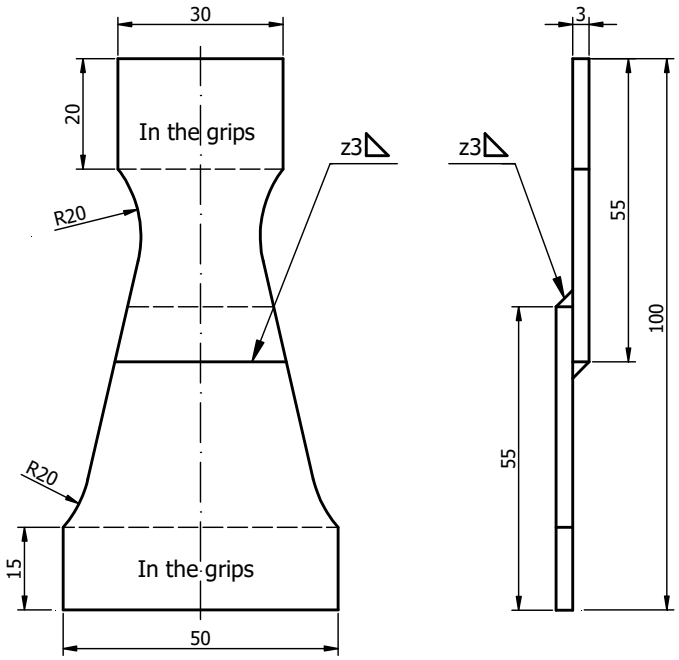
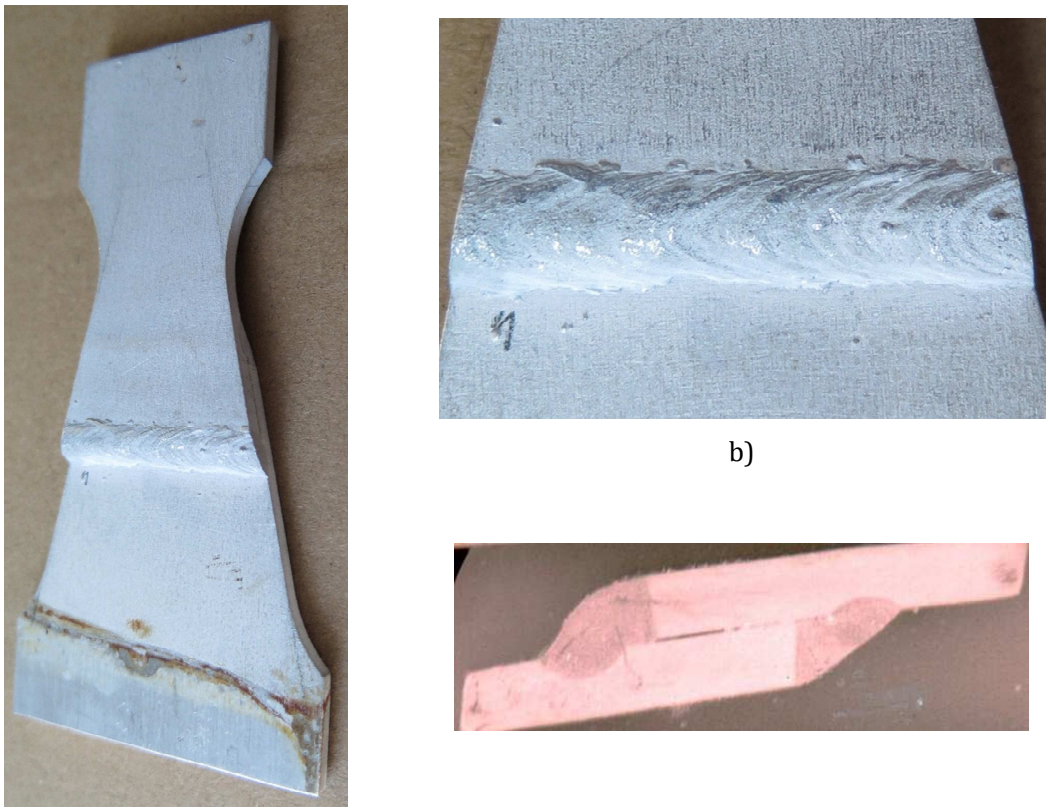


Fig. 1 *The lap-welded specimen (dimensions in mm)*



a) b) c)

Fig. 2 *a) Corroded lap-welded specimen; b) Detail of the specimen near the weld seam; c) Macrostructure of the lap-welded specimen*

Table 2 *Surface roughness of the uncorroded and corroded lap-welded specimens*

Roughness parameter[1]	*Parent metal zone*[2]					*Heat effected zone*[2]				
	X	*S*	*R*	*MX*	*MN*	*X*	*S*	*R*	*MX*	*MN*
	Uncorroded lap-welded specimens									
Ra (μm)	*0.14*	*0.00*	*0.01*	*0.14*	*0.14*	*4.66*	*0.12*	*0.21*	*4.74*	*4.52*
Rz (μm)	*0.86*	*0.01*	*0.02*	*0.87*	*0.85*	*24.99*	*8.07*	*14.29*	*29.97*	*15.58*
	Corroded lap-welded specimens									
Ra (μm)	*5.32*	*0.20*	*0.40*	*5.51*	*5.10*	*8.29*	*0.83*	*1.62*	*9.21*	*7.59*
Rz (μm)	*31.32*	*1.51*	*2.85*	*33.02*	*30.17*	*44.77*	*3.69*	*6.8*	*49.03*	*42.45*

[1] *Ra - arithmetical mean deviation of the profile*
Rz - maximum height of the profile

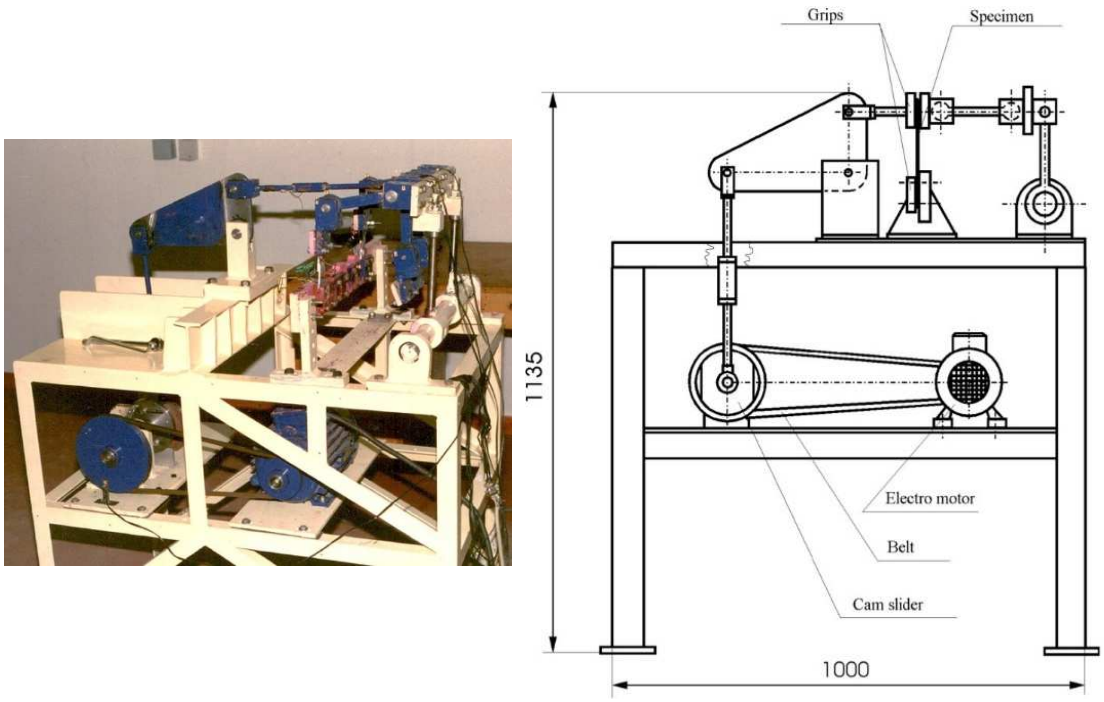
[2] *X – mean value of measurement*
S – estimated standard deviation
R – value measurement range
MX – maximum measurement value
MN - minimum measurement value

As a result of the accelerated corrosion test, roughness parameters in the parent metal zone increased 37-fold, while in the heat-affected zone (HAZ) they increased 1.8-fold. A maximum pit depth of approximately 0.2 *mm* was measured in the HAZ. The surface roughness of aluminium alloy 5083 also increases over time when exposed to seawater due to corrosion. Literature reports that pit depths in alloy 5083 reach approximately 0.18 *mm* after 5 years and between 0.6 and 0.9 *mm* after 10 years, depending on exposure conditions. However, quantitative long-

term roughness data, such as the arithmetical mean deviation of the profile (*Ra*) or the maximum height of the profile (*Rz*), are rarely reported. Most studies focus on corrosion rate, pitting depth, or loss of mechanical properties rather than direct surface roughness measurements. Therefore, a direct correlation between accelerated tests and long-term seawater exposure cannot be established. Accelerated tests can indicate relative susceptibility to pitting but do not fully replicate the complex corrosion mechanisms and changes in surface morphology observed during extended marine exposure. Nevertheless, the ferric chloride test remains a practical tool for engineering assessments, providing insight into the type and severity of corrosion damage that may occur in aluminium alloy 5083 during long-term marine service.

3. EXPERIMENTAL PROCEDURE

The fatigue test machine is driven by an electric motor through a belt transmission and enables the simultaneous testing of four specimens, as shown in Figure 3. Each specimen is rigidly clamped in the grips using screws, securing the lower part. The displacement amplitude at the specimen tip is controlled by adjusting the cam–slider eccentric mechanism, subjecting the specimens to cyclic bending under a constant stress ratio of −1.



a) b)

Fig. 3 *Custom-built fatigue testing machine: (a) photograph; (b) technical drawing (dimensions in mm)*

Bending tests were performed on uncorroded specimens (n = 22) at three load intensities and on corroded specimens (n = 8) at two load intensities. The cyclic displacement of the specimen's upper end represents the fatigue load at a constant level. The displacement recorded by the micrometer corresponds to the specimen's displacement at a point 3 *mm* below the upper edge of the grip.

The fracture locations, labelled 1 and 2, are shown in Figure 4a. Fractures occurred in the heat-affected zone at the weld toe, where the geometric features of the specimens caused increased local stress concentrations (Figures 4b and 4c). Visual examination of the fracture surfaces

consistently showed that crack initiation originated at the weld toe. From this point, an initial fatigue crack developed, propagated through the full plate thickness, and ultimately resulted in complete fracture (Figure 4d).

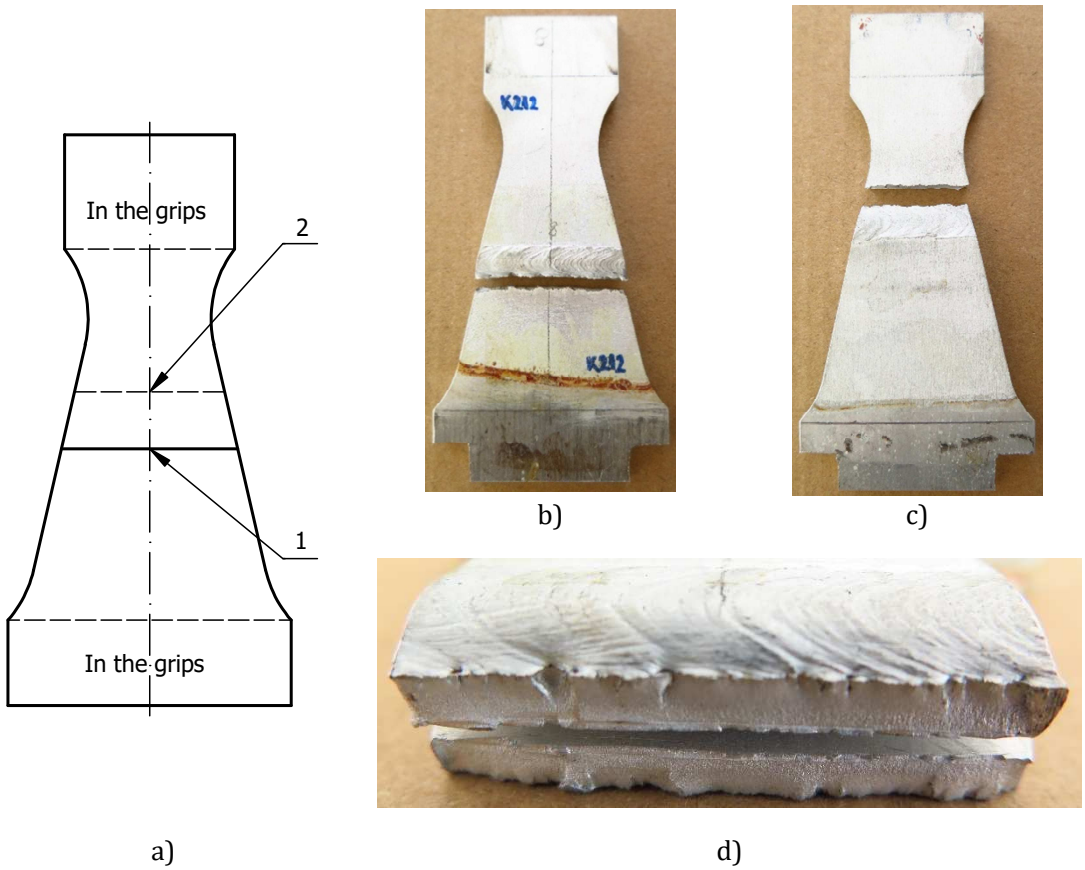


Fig. 4 *a) Fatigue fracture locations; b) Fractured specimen – location 1; c) Fractured specimen – location 2; d) Fractured surfaces – location 1*

4. STRESS CALCULATION

The experimental stress analysis was performed using two strain gauges (type 1.5/120 LY11) manufactured by Hottinger Baldwin Messtechnik. The strain gauges were positioned 1.8 *mm* from the weld toes. Their placement, orientation, and labelling are shown in Figure 5.

Finite element method (FEM) analysis was performed using the commercial software ANSYS 17.0. Tetrahedral elements with ten nodes (SOLID187 - quadratic shape function, 4-point Gaussian integration) were used in the finite element models. Material properties included a modulus of elasticity of 72 *GPa* and a Poisson's ratio of 0.33. A load was applied to the upper boundary surface, while the section corresponding to the lower grips was fully restrained to prevent displacement (Figure 6).

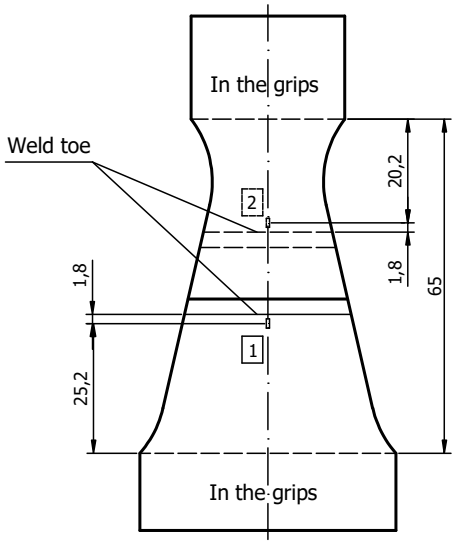


Fig. 5 *Placement, orientation, and labelling of the strain gauges (dimensions in mm)*

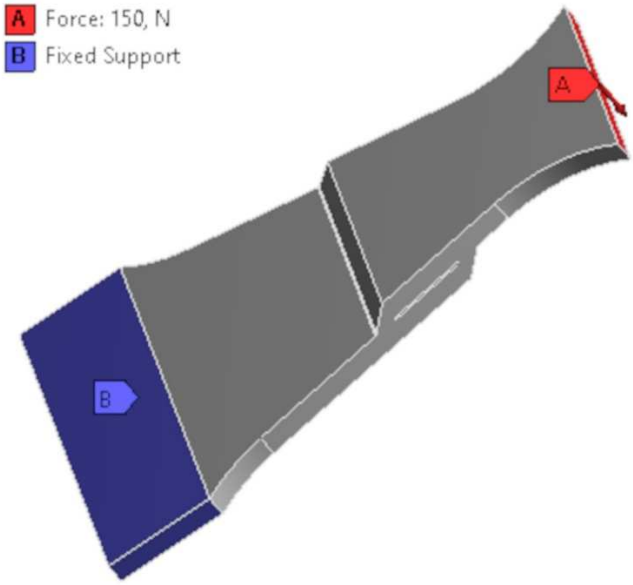


Fig. 6 *The boundary conditions and applied force location*

Nominal stress values were calculated according to the theory of elastic beams:

$$\sigma_n = F \cdot x / W(x) \quad \textbf{(2)}$$

where F is the applied force corresponding to a given displacement, x is the distance between the load application point and the fatigue failure location (38 mm and 22 mm at weld toe locations 1 and 2, respectively), and $W(x)$ is the elastic section modulus of the fracture surface (48.18 mm^3 and 36.74 mm^3 at weld toe locations 1 and 2, respectively).

The nominal stress values calculated using this approach closely match those obtained from strain gauge measurements and FEM analysis, indicating strong agreement between analytical and experimental methods. It should be noted that the strain gauges were positioned too far from the weld toes to be affected by stress concentrations. This consistency between FEM and

experimental results confirms the correct application of boundary conditions in the finite element model.

The stress distribution at various locations of the welded specimen, including the weld region where the fracture occurred, was determined using the finite element method. The notch stress concentration factor, K_t, was calculated based on a finite element model of the welded specimen, considering two weld reference radii: 0.3 *mm* and 0.05 *mm*.

In accordance with IIW guidelines [22], the finite element mesh was progressively refined towards the notch region to ensure accurate stress representation. The mesh resolution was required to satisfy the condition that the element size be smaller than one quarter of the selected reference radius (r_{ref} /4). Stress calculations were based on nodal stresses rather than element stresses. In this study, a finer mesh with element sizes of r_{ref} /5 in the notch region was used for both reference radii.

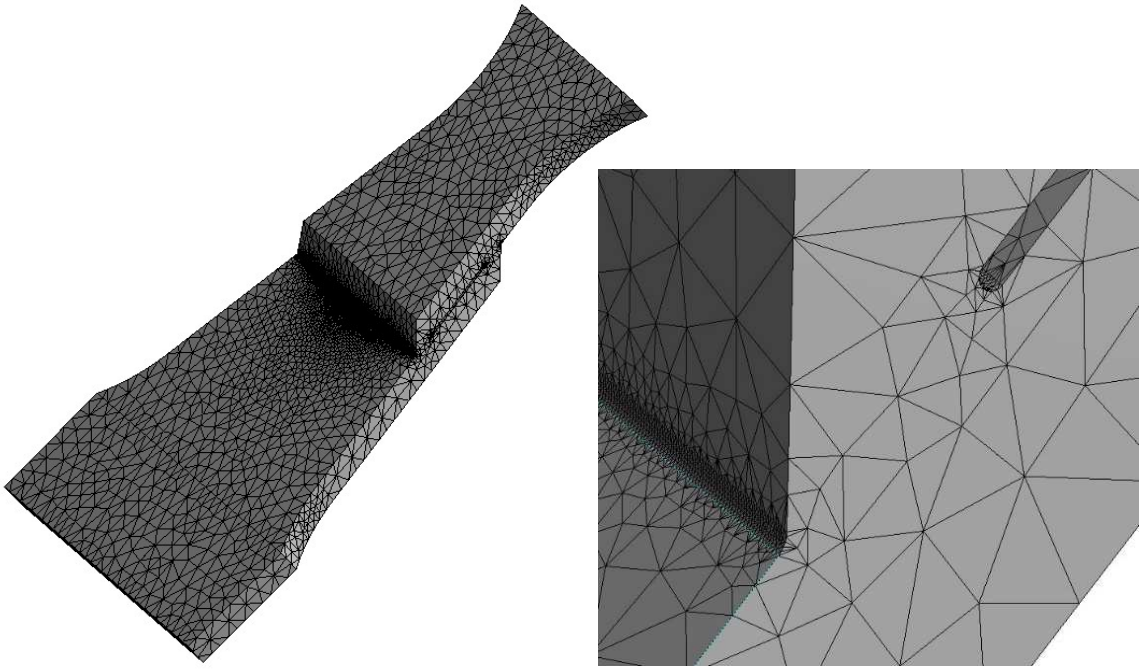
For the model with a reference radius of 0.3 *mm*, the minimum element edge length was 0.241 mm, resulting in a mesh with 948163 nodes and 618919 elements. For the model with a reference radius of 0.05 *mm*, the minimum element edge length was $4.017 \cdot 10^{-2}$ *mm*, and the mesh contained 1887818 nodes and 1261618 elements. To verify the reliability of the calculated notch stresses, a mesh convergence analysis was performed (Table 3).

Table 3 *Mesh convergence analysis results for the finite element model with a reference radius of 0.3 mm*

Solution number	*Maximum principal stress [MPa]*	*Change [%]*	*Nodes*	*Elements*
1	*281.96*		*948163*	*618919*
2	*279.07*	*-1.0309*	*1326986*	*883985*
3	*279.11*	$1.186 \cdot 10^{-2}$	*3258699*	*2269641*

The results showed no significant deviation from those obtained using the mesh with an element size of r_{ref} /5, confirming that further mesh refinement had a negligible effect on the calculated stress values. After the convergence study, the number of elements in the model increased from 618919 to 2269641 (more than a 3.6-fold increase), while the difference in the maximum principal stress was limited to approximately 1%.

The detailed configurations of the finite element models for the lap-welded specimen with rounded weld toe geometry are shown in Figure 7.



a) b)

Fig. 7 *a) Finite element model of a lap- welded specimen, r_{ref} = 0.3 mm; b) Detail of the mesh at the weld toe*

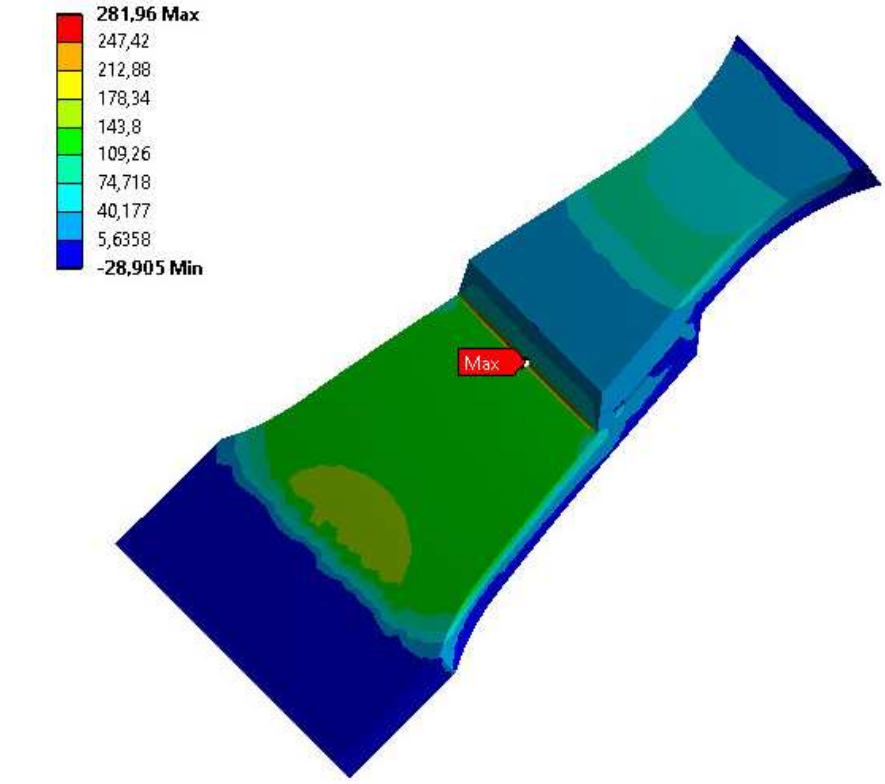
5. RESULTS AND ANALYSIS

5.1 STRESS RESULTS

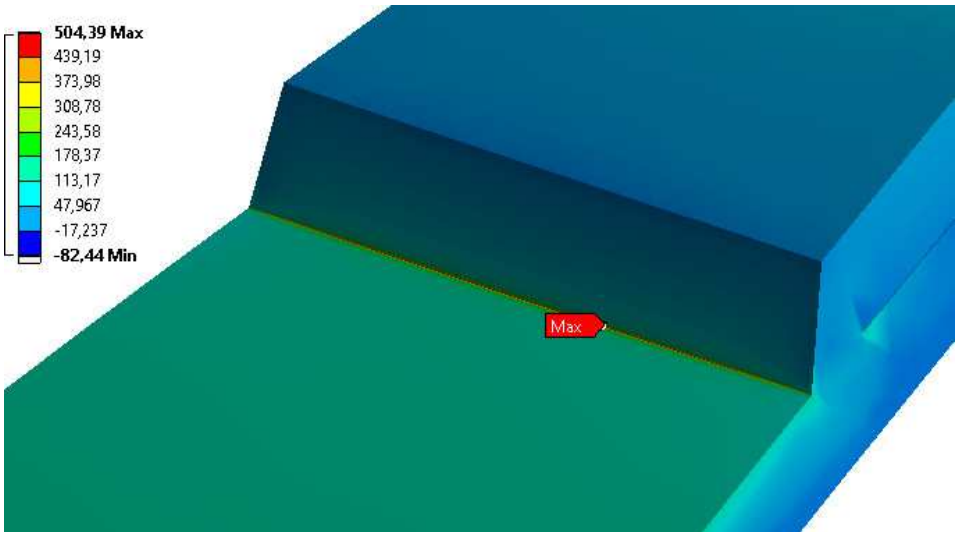
The distribution of the maximum principal stress under an applied force of $F = 150\ N$ on the upper boundary surface of the FEM model (Figure 6) is shown in Figure 8. Under this loading, a displacement of 1.8 *mm* occurs at the upper edge of the model in the direction of the applied force. The corresponding stress values, including the nominal stress (σ_n), the notch stress (σ_k), and the calculated notch stress concentration factor (K_t) at the fatigue fracture locations, are summarised in Table 4.

Table 4 *Nominal stress (σ_n), notch stress (σ_k), and notch stress concentration factor (K_t) for F = 150 N*

	σ_n [MPa]	σ_k (r_{ref} = 0.3 mm) [MPa]	σ_k (r_{ref} = 0.05 mm) [MPa]	K_t (r_{ref} = 0.3 mm)	K_t (r_{ref} = 0.05 mm)
Fatigue fracture location 1	*118.30*	*281.96*	*504.39*	*2.38*	*4.26*
Fatigue fracture location 2	*89.83*	*216.42*	*388.26*	*2.41*	*4.32*



a)



b)

Fig. 8 *Maximum principal stress distribution for F = 150 N at fatigue fracture location 1: a) r_{ref} = 0.3 mm, b) r_{ref} = 0.05 mm*

5.2 FATIGUE STRESS RESULTS

Fatigue tests were carried out on uncorroded and corroded specimens under three imposed cyclic displacement levels at the upper end of the specimen (1.8 *mm*, 1.2 *mm*, and 0.75 *mm*). The corresponding force intensities, determined by finite element analysis, were 150 *N*, 100 *N*, and 62.5 *N*, respectively. Nominal stress amplitudes were calculated using these force levels and Equation (2). As the specimens were tested at a stress ratio of $R = -1$, the influence of the stress ratio on fatigue strength was considered. According to the IIW recommendations [25], the proposed stress design curves apply to stress ratios $R \geq 0.5$, whereas for stress ratios $R < 0.5$, a fatigue increase factor $f(R)$ should be applied by multiplying the fatigue class of the classified detail. The fatigue increase factor depends on the magnitude and sign of the residual stresses. Assuming low residual stresses in the analysed specimens, Equation (1) was used to assign a fatigue increase factor of $f(R) = 1.3$ for a stress ratio of $R = -1$. Accordingly, the applied fatigue stresses at $R = -1$ were reduced by a factor of 1.3 (23.1%) to obtain stresses comparable to those at a stress ratio of $R = 0.5$. The nominal stress range and notch stress range at $R = 0.5$ were then determined using the nominal stress amplitudes, the notch stress concentration factors at fatigue fracture locations 1 or 2, and Eq. (1). The resulting values are summarised in Tables 5 and 6.

A total of 22 uncorroded and 8 corroded lap-welded specimens were subjected to fatigue testing. The number of specimens was determined based on the experimental objectives, test duration, and specimen availability. A larger number of uncorroded specimens (22) was tested to establish a reliable reference for fatigue behaviour and to capture the inherent scatter typically associated with fatigue life data. These data were required to construct statistically meaningful S–N curves for the uncorroded condition.

The number of corroded specimens (8) was limited because the corroded tests were intended to quantify the relative reduction in fatigue strength due to corrosion, rather than to establish a fully statistical S–N curve. Nevertheless, the selected number of corroded specimens was sufficient to identify clear trends and to enable direct comparison with the uncorroded reference data.

The fatigue test data were statistically analysed in accordance with ISO guidelines [28]. Fatigue life was evaluated using both the nominal stress method and the notch stress approach. The results were compared with the corresponding design S–N curves.

Table 5 *Fatigue test data for uncorroded lap-welded specimens*

Uncorroded specimen[1]	*Displacement of the specimen upper end, mm*	*Nominal stress amplitude[2] (R=-1), MPa*	*Nominal stress range[2], (R=0.5), MPa*	*Notch stress range[2], r_{ref}=0.3 mm, (R=0.5), MPa*	*Notch stress range[2], r_{ref}=0.05 mm, (R=0.5), MPa*	*Number of cycles to failure*	*Fatigue fracture location*
10	*1.8*	*90*	*138.5*	*333.7*	*598.2*	*83000*	*2*
11		*90*	*138.5*	*333.7*	*598.2*	*93000*	*2*
12		*90*	*138.5*	*333.7*	*598.2*	*175000*	*2*
13		*118*	*181.5*	*432.1*	*773.4*	*200000*	*1*
14		*118*	*181.5*	*432.1*	*773.4*	*246000*	*1*
15		*90*	*138.5*	*333.7*	*598.2*	*63000*	*2*
20	*1.2*	*60*	*92.3*	*222.5*	*398.8*	*452000*	*2*
21		*60*	*92.3*	*222.5*	*398.8*	*364000*	*2*
22		*60*	*92.3*	*222.5*	*398.8*	*700000*	*2*
23		*60*	*92.3*	*222.5*	*398.8*	*280000*	*2*
24		*60*	*92.3*	*222.5*	*398.8*	*982000*	*2*
25		*79*	*121.5*	*289.3*	*517.8*	*1465000*	*1*
30	*0.75*	*49*	*75.4*	*179.4*	*321.1*	*1067200*	*1*
31		*49*	*75.4*	*179.4*	*321.1*	*1182850*	*1*
32		*37.5*	*57.7*	*139.0*	*249.2*	*1556320*	*2*
33		*37.5*	*57.7*	*139.0*	*249.2*	*2110330*	*2*
34		*49*	*75.4*	*179.4*	*321.1*	*2351370*	*1*
35		*37.5*	*57.7*	*139.0*	*249.2*	*2910910*	*2*
36		*37.5*	*57.7*	*139.0*	*249.2*	*3217850*	*2*
37		*37.5*	*57.7*	*139.0*	*249.2*	*4535740*	*2*
38		*49*	*75.4*	*179.4*	*321.1*	*4992230*	*1*
39		*37.5*	*57.7*	*139.0*	*249.2*	*6068850*	*2*

[1] Specimen designation AB: A - displacement level; B – specimen number at the specified displacement level
[2] Defined at the fatigue fracture location

Table 6 *Fatigue test data for corroded lap-welded specimens*

Corroded specimen[1]	*Displacement of the specimen upper end, mm*	*Nominal stress amplitude[2] (R=-1), MPa*	*Nominal stress range[2], (R=0.5), MPa*	*Notch stress range[2], r_{ref}=0.3 mm, (R=0.5), MPa*	*Notch stress range[2], r_{ref}=0.05 mm, (R=0.5), MPa*	*Number of cycles to failure*	*Fatigue fracture location*
10	*1.8*	*90*	*138.5*	*333.7*	*598.2*	*30500*	*2*
11		*118*	*181.5*	*432.1*	*773.4*	*26030*	*1*
12		*90*	*138.5*	*333.7*	*598.2*	*32560*	*2*
13		*90*	*138.5*	*333.7*	*598.2*	*39810*	*2*
20	*1.2*	*60*	*92.3*	*222.5*	*398.8*	*137940*	*2*
21		*79*	*121.5*	*289.3*	*517.8*	*112530*	*1*
22		*60*	*92.3*	*222.5*	*398.8*	*99200*	*2*
23		*79*	*121.5*	*289.3*	*517.8*	*70230*	*1*

[1] Specimen designation AB: A displacement level; B – specimen number at the specified displacement level
[2] Defined at the fatigue fracture location

The following S–N curve equations, corresponding to a survival probability Ps = 97.7%, together with the associated stress scatter ranges – defined as T_σ = 1:($\Delta\sigma(Ps$ = 10%$)$ / $\Delta\sigma(Ps$ = 90%$)$) - were derived:

- Nominal stress approach:
  - For uncorroded lap-welded specimens (FAT40), the relationship is:

$$logN = 11.180 - 3.050 \cdot log\Delta\sigma_k;\ T_\sigma = 1:1.915 \quad \textbf{(3)}$$

  - For corroded lap-welded specimens (FAT20):

$$logN = 9.596 - 2.560 \cdot log\Delta\sigma_k;\ T_\sigma = 1:1.410 \quad \textbf{(4)}$$

- Notch-stress approach:
  a) For the reference radius r_{ref} = 0.3 *mm*:
     - Uncorroded lap-welded specimens (FAT97):

$$logN = 12.421 - 3.080 \cdot log\Delta\sigma k;\ T_\sigma = 1:1.884. \quad \textbf{(5)}$$

     - Corroded lap-welded specimens (FAT60)

$$logN = 10.958 - 2.618 \cdot log\Delta\sigma_k,;\ T_\sigma = 1:1.380 \quad \textbf{(6)}$$

  b) For the reference radius r_{ref} = 0.05 *mm*:
     - Uncorroded lap-welded specimens (FAT174):

$$logN = 13.212 - 3.084 \cdot log\Delta\sigma_k,;\ T_\sigma = 1:1.377 \quad \textbf{(7)}$$

     - Corroded lap-welded specimens (FAT108)

$$logN = 11.641 - 2.625 \cdot log\Delta\sigma_k;\ T_\sigma = 1:1.243 \quad \textbf{(8)}$$

The S–N curves corresponding to a survival probability of 97.7% for both corroded and uncorroded specimens are shown in Figures 9–11. Figure 9 presents the results obtained using the nominal stress approach, while Figures 10 and 11 show the results of the notch stress method with reference radii of 0.3 *mm* and 0.05 *mm*, respectively, along with the corresponding design S–N curves.

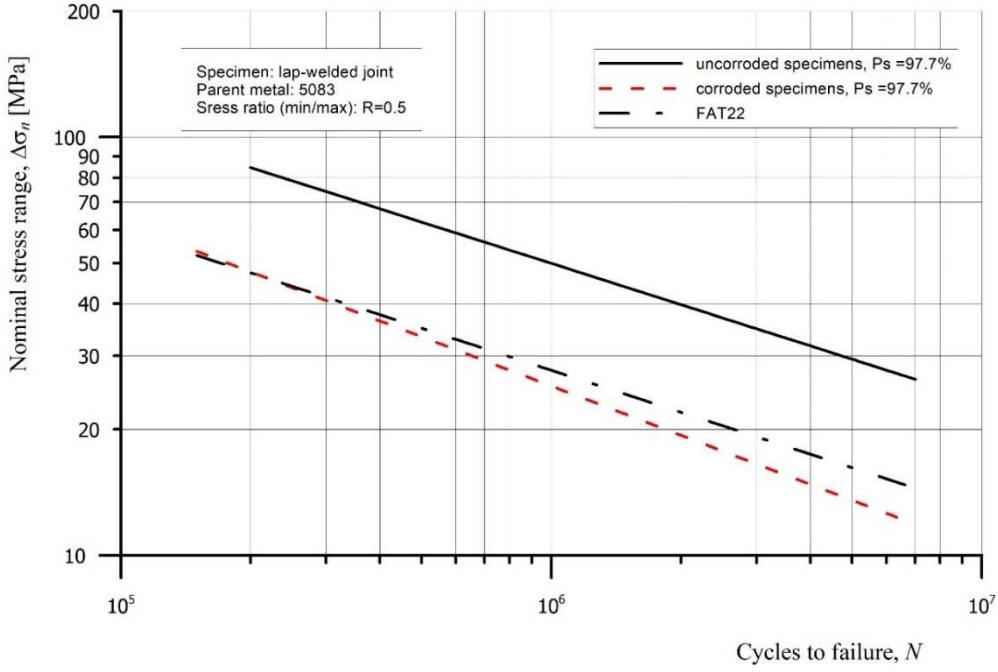


Fig. 9 *S–N curves for corroded and uncorroded lap-welded specimens, compared with the nominal stress design curve FAT22*

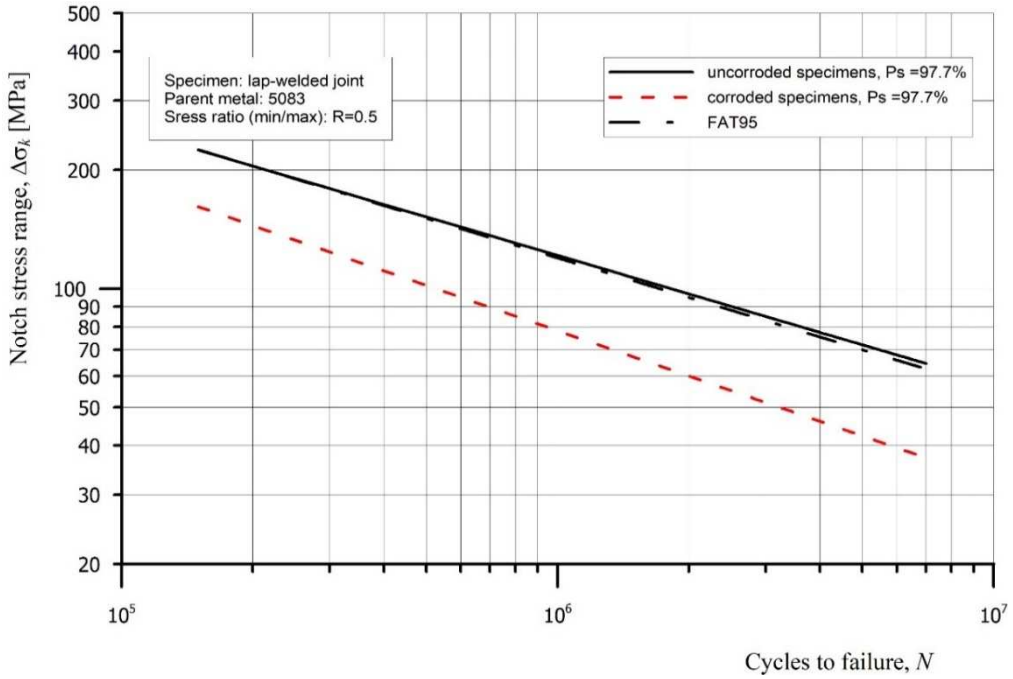


Fig. 10 *S–N curves for corroded and uncorroded lap-welded specimens, compared with the notch stress design curve FAT95 (r_{ref} = 0.3 mm)*

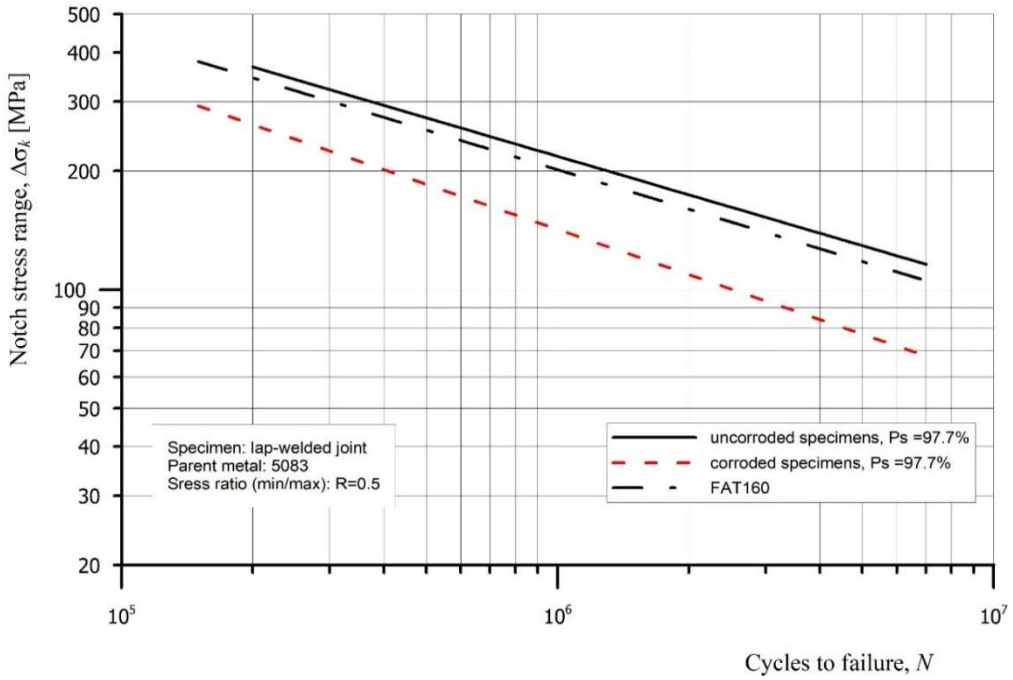


Fig. 11 *S–N curves for corroded and uncorroded lap-welded specimens, compared with the notch stress design curve FAT160 (r_{ref} = 0.05 mm)*

Comparison of the stresses at $N_{ref} = 2 \cdot 10^6$ cycles, obtained from the design S–N curves and the fatigue tests (survival probability Ps = 97.7%), shows the following:

- Using the nominal stress approach, the FAT22 design curve is conservative. The difference between the fatigue test stress range and the design S–N curve stress range is 82%.

- Using the notch stress approach with r_{ref} = 0.3 *mm*, the fatigue stress ranges are nearly identical, with a difference of only 2%.
- Using the notch stress approach with r_{ref} = 0.05 *mm*, the difference between the fatigue test stress range and the design S–N curve stress range is 9%.

Comparison of fatigue stress ranges at $N_{ref} = 2 \cdot 10^6$ cycles between uncorroded and corroded specimens indicates:

- For the nominal stress approach, the fatigue stress range of corroded specimens is 50% lower than that of uncorroded specimens.
- For the notch stress approach with r_{ref} = 0.3 *mm*, the fatigue stress range of corroded specimens is 38.1% lower than that of uncorroded specimens.
- For the notch stress approach with r_{ref} = 0.05 *mm*, the fatigue stress range of corroded specimens is 37.9% lower than that of uncorroded specimens.

The observed reduction in fatigue strength of corroded specimens can be attributed to increased surface roughness and the presence of corrosion-induced pitting, particularly in the heat-affected zone.

6. DISCUSSION AND CONCLUSION

Although aluminium alloys generally exhibit good corrosion resistance, welded components and structures require careful design for use in corrosive environments. The fatigue behaviour of aluminium alloy welded joints can be evaluated using the S–N curve method, with the choice of an appropriate FAT design curve depending on the stress definition applied. In this study, fatigue analysis was performed using both the nominal stress and notch stress approaches. Two variants of the notch stress approach were applied, both suitable for joints made from 3 *mm* thick plates. Comparison of fatigue test results for uncorroded specimens with the corresponding design S–N curves shows that the notch stress approach provides a more accurate assessment of allowable stress ranges. In particular, the variant with a reference radius r_{ref} = 0.3 *mm* and a FAT95 design curve produced fatigue stress ranges closely matching experimental results, with a deviation of only 2%. The approach using r_{ref} = 0.05 *mm* and FAT160 also yielded satisfactory results, with a deviation of 9% between the test data and the design S–N curve.

Design guidelines for steel and aluminium alloy welded joints generally assume a non-corrosive service environment with adequate protection against atmospheric corrosion. Structures exposed to corrosive environments or lacking sufficient protection require a reduction in the fatigue strength class. The extent of this reduction depends on the fatigue stress range and the duration of environmental exposure. For steel structures (excluding stainless steels used in marine environments), the IIW recommends limiting applied fatigue strength to 70% of standard values; however, no specific guidance currently exists for aluminium alloys.

Previous studies investigating the influence of corrosion on the fatigue behaviour of welded aluminium alloys show considerable methodological diversity. Pre-corrosion exposure durations range from 10 to 1000 hours, with most studies using a 3.5% NaCl solution. These investigations have primarily focused on friction stir-welded 2024-T3 aluminium alloy joints and indicate that corrosion adversely affects fatigue behaviour. However, they do not provide a quantitative relationship between the degree of corrosion damage and the corresponding reduction in fatigue strength under cyclic loading. Moreover, for homogeneous 5083 fillet-

welded joints subjected to pre-corrosion, no direct quantitative comparisons of fatigue life have been reported, highlighting a significant gap in the literature for this material and exposure condition.

The results of the present study, obtained by comparing fatigue tests on uncorroded and corroded specimens, indicate that the fatigue class of uncorroded welded joints should be reduced by approximately 50% when using the nominal stress approach and by 38% when using the notch stress approach. This reduction is primarily attributed to the detrimental effects of corrosion, including increased surface roughness and the formation of corrosion pits, which accelerate crack initiation and reduce fatigue life.

A key challenge remains in correlating laboratory test results with the behaviour of real structural components in marine environments. The relationship between surface damage caused by natural marine corrosion and that induced by standardised pre-corrosion tests is still unclear. Further research is required to establish correlations between marine exposure duration, the resulting surface damage (such as pitting and surface roughness changes), and the associated reduction in fatigue strength of aluminium alloy welded joints.

7. REFERENCES

[1] International Aluminium Institute, *Primary Aluminium Production Statistics*. International Aluminium Institute, dataset, 2024.

[2] Hirsch, T., Al-Samman, T., Superior light metals by texture engineering: Optimized aluminum and magnesium alloys for automotive applications, *Acta Materialia*, Vol. 61, No. 3, pp. 818-843, 2013. https://doi.org/10.1016/j.actamat.2012.10.044

[3] Jin, H., Optimization of Aluminum Alloy AA5083 for Superplastic and Quick Plastic Forming, *Metallurgical and Materials Transactions A*, Vol. 50, pp. 3868–3890, 2019.

https://doi.org/10.1007/s11661-019-05305-x

[4] IACS, *Unified Requirement UR W25: Aluminium Alloys for Hull Construction and Marine Structure*; Rev.6; International Association of Classification Societies: London, UK, 2021.

[5] ASM International, *Properties and selection: nonferrous alloys and special-purpose materials*, 10th ed. Ohio (Metal Park): ASM Handbook. 1990.

[6] Ailor, W.H., Ten-Year Seawater Tests on Aluminum (Chapter), *Corrosion in Natural Environments*, eds. Ailor, W.H., Dean, S. W., Haynie, F. H., ASTM International, 18 pages, 1974. https://doi.org/10.1520/STP32161S

[7] Nwoye, C., Neife, S., Ameh, E., Nwobasi A., Idenyi, N., Predictability of Al-Mn Alloy Exposure Time Based on Its As-Cast Weight and Corrosion Rate in Sea Water Environment, *Journal of Minerals and Materials Characterization and Engineering*, Vol. 1, No. 6, pp. 307-314, 2013. http://dx.doi.org/10.4236/jmmce.2013.16046

[8] Le, L., Severe Corrosivity and Its Eletrochemical Mechanism of Seawater in Xiamen Sea Area to Al-Mg Alloys, *Journal of Electrochemistry*, Vol. 9, No. 3, Article 13, 2003.

https://doi.org/10.61558/2993-074X.3314

[9] Goddard, H.P., Jepson, W.B., Bothwell, M.R., Kane, R.L., *The Corrosion of Light Metals*, John Wiley and Sons, New York, USA, 1967.

[10] Pantelakis, S., Kermanidis, A., Effect of Corrosion on the Mechanical Behaviour of Aircraft Aluminium Alloys (Chapter), *Corrosion Control in the Aerospace Industry*, eds. Benavides, S., Woodhead Publishing Series in Metals and Surface Engineering, pp. 67-108, 2009.

https://doi.org/10.1533/9781845695538.1.67

[11] Heuler, P., Birk, O., Durability Assessment of Automotive Aluminium Parts, *Fatigue & Fracture of Engineering Materials & Structures*, Vol. 25, No. 12, pp. 1135-1148, 2002.

http://dx.doi.org/10.1046/j.1460-2695.2002.00590.x

[12] Ghidini, T., Alfaro, U., Donne, C., Fatigue Life of Friction Stir Welded Joints in the Presence of Corrosion Damage: Experiments and Calculations, *Materials Testing*, Vol. 47, No. 7-8, pp. 456-461, 31 DVM Conference, BMW Forschung- und Innovationszentrum, München, 2005. https://doi.org/10.3139/120.100681

[13] Yadav, V., Gaur, V., Singh, I., Effect of Pre-Corrosion on Crack Initiation Behavior of Friction Stir Welded Aluminum Alloy 2024-T3 in High and Low Cycle Fatigue Regimes, *International Journal of Fatigue*, Vol. 179, No. 3, Article 108037, 2023.

https://doi.org/10.1016/j.ijfatigue.2023.108037

[14] Ghidini, T., Donne, C., Mercado, U.A., Predicting the Fatigue Life of Pristine and Pre-corroded Friction Stir Welded Joints, *International Journal of Structural Integrity*, Vol. 2, No. 2, pp. 200-213, 2011. https://doi.org/10.1108/17579861111135932

[15] Ghidini, T., Alfaro, U., Donne, C., Fatigue Life of Friction Stir Welded Joints in the Presence of Corrosion Damage: Experiments and Calculations, *Materials Testing*, Vol. 47, No. 7-8, pp. 456-461, 2005. https://doi.org/10.3139/120.100681

[16] Wu, H., Chen, Y., Lu, D., He, G., Effect of Corrosion Environment on Mechanical Behavior of 5083/6005A Welded Joints, *Metals*, Vol. 14, No. 8, Article 925, 2024.

https://doi.org/10.3390/met14080925

[17] Chen, Y., Wu, H., Wang, X., Zeng, X., Huang, L., Gu, H., Li, H., Corrosion Mechanism and the Effect of Corrosion Time on Mechanical Behavior of 5083/6005A Welded Joints in a NaCl and $NaHSO_3$ Mixed Solution, *Crystals*, Vol. 12, No. 8, Article 1150, 2022.

https://doi.org/10.3390/cryst12081150

[18] Jie, Z., Wang, W., Zhuge, P., Li, Y., Wei, X., Fatigue properties of inclined cruciform welded joints with artificial pits, *Advanced Steel Construction*, Vol. 17, No. 1, pp. 20-27, 2021.

http://dx.doi.org/10.18057/IJASC.2021.17.1.3

[19] EN 1999-1-3, *Eurocode 9: Design of Aluminium Structures—Part 1–3: Structures Susceptible to Fatigue*, CEN: Brussels, Belgium, 2011.

[20] Hobbacher, A.F., Baumgartner, J., *Recommendations for Fatigue Design of Welded Joints and Components*, 3rd ed., Springer: Cham, Switzerland, 2024.

https://doi.org/10.1007/978-3-031-57667-6

[21] Rennert, R., Kullig, E., Vormwald, M., Esderts, A., Siegele, D., *FKM Guideline: Analytical Strength Assessment of Components Made of Steel, Cast Iron and Aluminum Materials in Mechanical Engineering*, 6th ed., VDMA, Frankfurt, Germany, 2012.

[22] Fricke, W., *IIW Recommendations for the Fatigue Assessment of Welded Structures by Notch Stress Analysis: IIW-2006-09*, Woodhead Publishing Limited, Cambridge, UK, 2012.

https://doi.org/10.1533/9780857098566

[23] Baumgartner, J., Review and considerations on the fatigue assessment of welded joints using reference radii, *International Journal of Fatigue*, Vol. 101, No. 2, pp.459–468, 2017.

https://doi.org/10.1016/j.ijfatigue.2017.01.013

[24] Baumgartner, J., Hobbacher, A.F., Rennert, R., Fatigue assessment of welded thin sheets with the notch stress approach - Proposal for recommendations, *International Journal of Fatigue*, Vol. 140, No. 12, Article 105844, 2020.

http://dx.doi.org/10.1016/j.ijfatigue.2020.105844

[25] Bertil Jonsson, Dobmann, G., Hobbacher, A.F., Kassner, M., Marquis, G., *IIW Guidelines on Weld Quality in Relationship to Fatigue Strength*, Springer: Cham, Switzerland, 2016.

https://doi.org/10.1007/978-3-319-19198-0

[26] EN 1011-4:2000, *Welding—Recommendations for Welding of Metallic Materials—Part 4: Arc Welding of Aluminium and Aluminium Alloys*, CEN: Brussels, Belgium, 2000.

[27] ISO 10042:2018, *Welding—Arc-Welded Joints in Aluminium and Its Alloys—Quality Levels for Imperfections*, ISO: Geneva, Switzerland, 2018.

[28] ISO/TR 14345:2012, *Fatigue—Fatigue Testing of Welded Components—Guidance*, ISO: Geneva, Switzerland, 2012.